Fate of Iron during Hydrothermal Liquefaction of Hemin

Jimeng Jiang, Joseph J. Serago, Kevin Torres, Emily Rapp, and Phillip E. Savage*
Department of Chemical Engineering,
Pennsylvania State University, University Park, PA 16802
psavage@psu.edu

Abstract

Hemin, an iron porphyrin, was used as a model compound to study the fate of iron during hydrothermal liquefaction (HTL). Hemin decomposed hydrothermally and produced an oil-phase with appreciable iron content only at temperatures exceeding 250 °C. Both the temperature of and the time in the hydrothermal environment affect the iron concentration in the oil from hemin HTL, with severe conditions leading to lower iron concentrations. Catalysts (Ni/Al_2O_3-SiO_2) and solvents (MTBE) that were effective in algal HTL biocrude demetallation also reduced iron concentrations in oil from hemin HTL. Iron porphyrinic species were identified in the oil from hemin HTL. They were much less prevalent when a Ni/Al_2O_3-SiO_2 catalyst was also used, which points to the effectiveness of catalytic HTL for demetallation of the oil. In addition, there were many species in the oil products with two nitrogen atoms, which formed from hemin decomposition.

1. Introduction

Hydrothermal liquefaction (HTL) uses chemical reactions in hot, compressed water near its critical point (374 °C) to convert wet biomass, including microalgae, into an energy-dense, crude bio-oil. HTL capitalizes on the combined effects of thermal energy, pressure, and hydrolytic attack of water molecules to decompose biomacromolecules into fragments that are typically < 1000 amu. One vision for integration of HTL into fuel production is to blend algae HTL biocrude with petroleum and process the mixture using existing refinery technology. A roadblock in realizing this vision is the high iron content of algae HTL biocrude. Iron is typically

the only transition metal present in algae HTL biocrude in concentrations exceeding 1000 ppm. [1,2], The presence of high concentrations of iron in biocrude could cause detrimental effects in a refinery, such as deposition and catalyst deactivation [3–7].

Recognizing the importance of limiting the iron content in algae HTL biocrude, we previously investigated the effects of different HTL processing conditions, solvents, and heterogeneous catalysts on the iron concentrations in biocrude [1,8] from algae. However, it is difficult to explore the demetallation reactions and identify iron-containing molecular products when working with actual microalgal biomass because of its complexity. To learn more about the hydrothermal reactions of iron-containing compounds, we sought to examine a model compound that mimics, to the extent possible, the iron-containing moieties in microalgae.

Key iron-containing components in microalgae are hemoproteins, which are involved in metabolic pathways such as oxygen sensing, electron transport, and signal transduction. [9–11] The prosthetic groups of the hemoproteins are hemes, which are porphyrinic speices with a central Fe atom. Heme b is the most abundant heme [10] and its molecular structure is shown in Figure 1. The nucleus of porphyrin molecules is a large cyclic structure composed of four pyrrole rings linked at their alpha positions by methene bridges. These four bridge (meso) positions are the most reactive sites in porphyrins.[12] The other eight peripheral (beta) positions are less reactive. A variety of reactions including nitration, [13] halogenation, [14] and oxidative cleavage [15] can occur at meso carbons.

Porphyrinic iron resides in algal HTL biocrude and Jarvis et al. [2] identified more than 100 unique iron porphyrin compounds. The iron porphyrin compounds have a distribution of carbon numbers and double bond equivalents (DBE) similar to the metal porphyrins (e.g., Ni and V) in petroleum. While removal of Ni and V from porphyrin compounds has been studied

extensively [16–20], there is scarce information about the fates of iron porphyrins during hydrothermal treatment.

Given the prevalence of iron porphyrin structures in both microalgae and the algal HTL biocrude oil, and the lack of information about the reactions of iron porphyrins during HTL, we used hemin (Fig. 1b) as a model compound to examine iron fates during HTL.

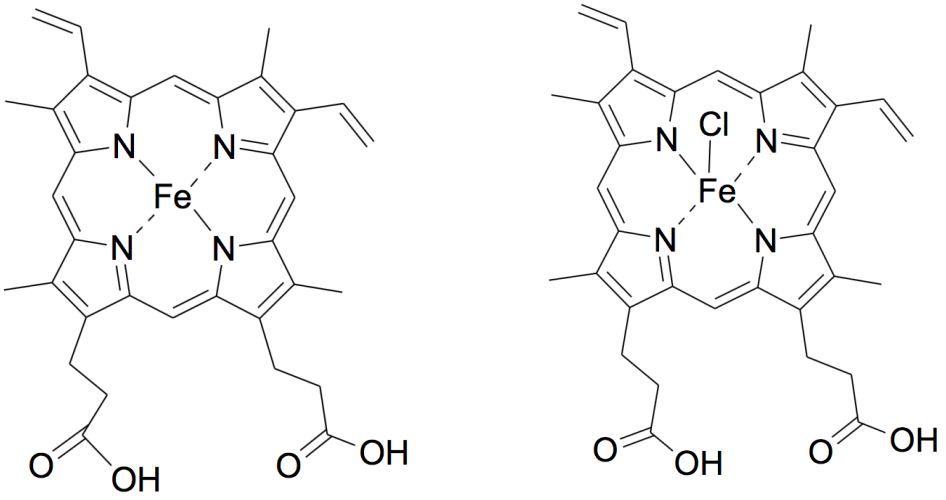

Figure 1: Structures of heme b (left) and hemin (right)

2. Materials and Methods

2.1 Materials

Hemin (porcine) was purchased from Alfa Aesar with 98+% purity. Dichloromethane (DCM), methyl-t-butyl ether (MTBE), and ethylene glycol butyl ether (EGBE) were HPLC grade with purity ≥ 99.5% and purchased from Sigma Aldrich. NaOH was purchased from Sigma Aldrich. Elemental Blank Oil was purchased from the Conostan Division, Continental Oil Company. The blank oil was 100% white mineral oil with a viscosity of 75 cSt. It consists of C9 – C16 hydrocarbons. An iron standard in an oil phase (FEOMS 1000 µg/mL iron in mineral oil)

was purchased from High-Purity Standards. Swagelok stainless steel caps and port connectors (nominal ½ in) were used to make 4.1 mL batch reactors.

Activated charcoal and ruthenium (5 wt%) on activated charcoal were obtained from Sigma-Aldrich as powders and used as received. Cobalt molybdenum oxide supported on alumina (3.4-4.5% cobalt oxide, 11.5-14.5% molybdenum oxide) was purchased from Alfa Aesar and ground into powder before use. Nickel on silica-alumina ((66±5)% nickel) was purchased as a powder from Alfa Aesar and used as received.

2.2 Procedure

3 wt% of hemin, 12 wt% of elemental blank oil (in most runs), a selected weight percent (12.5% -100% relative to hemin) of heterogeneous catalyst (in selected runs), and DI water (balance in all runs) were loaded into 4.1 mL batch mini reactors. The elemental blank oil does not contain any metals and its purpose is to facilitate the low loadings of hemin used herein and to ensure a dilution ratio of less than 100 when preparing post-HTL oil samples for analysis of iron. The reactors were then placed in a fluidized sand bath preheated to the desired set point temperature. All temperatures mentioned herein as HTL conditions refer to this set point temperature. After the desired holding time had elapsed, reactors were removed from the sand bath, quickly cooled to room temperature, and subjected to product recovery.

Product recovery follows the procedure described in a previous study. [1] In summary, DCM and MTBE were used as solvents to recover the post-HTL oil that is present. The solvent, in small aliquots, was added to the reactors until the material withdrawn from the reactor became clear. After centrifuging the mixture containing all of the reactor contents, the aqueous phase was

removed first and the solid phase was then filtered out. The remaining oil-containing organic phase was dried at 40 °C (DCM) or 45 °C (MTBE) to remove the solvent.

The solvent-free oil phase was then collected, prepared for analysis, and subjected to metal analysis using Inductively Coupled Plasma - Optical Emission Spectroscopy (ICP-OES) as described previously.[8] A dedicated organic sample introduction system was coupled to the ICP-OES. Oil samples and iron standards in mineral oil were diluted by EGBE as needed. Spent catalysts with the HTL solid products were characterized by SEM-EDS using a NanoSEM 630 (FEI, Hillsboro, OR) with the X-max detector (Oxford Instruments, Concord, MA) at 10 kV.

Products from hemin HTL with no added blank oil were collected using DCM as a recovery solvent and the same workup procedure and analyzed with a Shimadzu GC-MS QP-2010 Ultra with a 0.25 mm inner diameter Agilent DB-SMS column (30 m x 0.25 μm). The inlet temp was 200 °C, the flow rate was 2 mL/min, and the oven temperature program was 35 °C for 1 min with a subsequent ramp of 5.6 °C /min to 315 °C (final oven temperature). These samples were also analyzed by Fourier Transform Ion Cyclotron Resonance (FT-ICR) Mass Spectrometry (MS) at UC Berkeley. The procedures for sample preparation and FT-ICR MS operation were adapted from Jarvis et al. [2]

3. Results and Discussion

Table 1 summarizes the HTL reaction conditions and the resulting iron content in the oil phase. We added catalysts in several runs and explored the effect of different solvents for recovering the oil. Run 33 and Run 35 were control experiments.

Run 33 tested whether the blank oil and DI water together will leach any iron from the stainless steel reactor walls. This control experiment was conducted where no hemin was added to the reactor and it was

Table 1: Reaction conditions and iron content (ppm) in the hemin oil from HTL. Catalyst loading is relative to hemin loaded.

Run	Catalyst	Catalyst loading (%)	Solvent	Temp (°C)	Time (min)	Iron in oil (ppm)
1	N/A	N/A	DCM	200	60	29±21
2	N/A	N/A	DCM	250	60	14±10
3	N/A	N/A	DCM	300	60	1625
4	N/A	N/A	DCM	350	60	4974
5	N/A	N/A	DCM	400	3	3182±510
6	N/A	N/A	DCM	400	60	4262±240
7	N/A	N/A	DCM	400	80	2560
8	N/A	N/A	DCM	400	100	2760±360
9	N/A	N/A	MTBE	400	60	3301±512
10	AC	25	DCM	400	10	5696±1343
11	AC	25	DCM	400	30	4879±1006
12	AC	25	DCM	400	60	3080±690
13	AC	45	DCM	400	30	2476±125
14	AC	45	DCM	400	60	3060±111
15	AC	65	DCM	400	60	2727±372
16	AC	50	MTBE	400	60	1817±425
17	AC	100	MTBE	400	60	73±24
18	$CoMo/Al_2O_3$	15	DCM	400	60	3462±258
19	$CoMo/Al_2O_3$	25	DCM	400	30	3782±230
20	$CoMo/Al_2O_3$	25	DCM	400	60	3215±274
21	$CoMo/Al_2O_3$	25	MTBE	400	60	2308±158
22	$CoMo/Al_2O_3$	50	MTBE	400	60	1440±127
23	$CoMo/Al_2O_3$	100	MTBE	400	60	740±68
24	Ni/Al_2O_3-SiO_2	25	DCM	300	60	453±131
25	Ni/Al_2O_3-SiO_2	25	DCM	350	60	1894±81
26	Ni/Al_2O_3-SiO_2	10	DCM	400	60	1043±188
27	Ni/Al_2O_3-SiO_2	25	DCM	400	10	423
28	Ni/Al_2O_3-SiO_2	25	DCM	400	30	542
29	Ni/Al_2O_3-SiO_2	25	DCM	400	40	912±756
30	Ni/Al_2O_3-SiO_2	25	DCM	400	50	43±35
31	Ni/Al_2O_3-SiO_2	25	DCM	400	60	10
32	Ru/C	25	DCM	400	30	5608±717
33	N/A		DCM	400	60	2.5±1.9

34	N/A	DCM	25	60	29±9
35	N/A	DCM & NaOH	400	100	2863

AC represents activated charcoal

held at 400 °C for 60 min. The iron content of just 2.5 ppm in Run 33 demonstrates there is minimal iron leached from the reactor during the experiments. If all of the iron in hemin were transferred to the oil phase, the iron concentration would exceed 10,000 ppm.

Run 35 tested whether adding caustic will affect the iron content in product phases. In Run 35, the reactor received aliquots of 0.1 M NaOH solution after completion of the regular product recovery protocol that only used DCM as a recovery solvent. The intent of adding the NaOH solution is to dissolve any unreacted hemin and other undissolved organic matter and transfer it to the aqueous phase. This aqueous phase extracted by additional NaOH is much darker than the aqueous phase product obtained from HTL without added caustic, indicating that some solid products remained in the reactor and were solubilized in the NaOH solution. However, the iron content in the oil phase is not affected as the iron concentration in Run 35 (2863 ppm) is similar to that in Run 8 (2760 ppm). This result means that the solutes extracted in NaOH partition into the aqueous phase rather than the oil.

3.1 Effect of reaction temperature

Figure 2 shows the effect of reaction temperature on the iron content in the hemin oil from hydrothermal treatment for 60 min. Note the y-axis is a log scale. There is minimal iron (14-29 ppm) in the crude oil when hemin is in the hydrothermal medium at either 200 °C or 250 °C. Run 34 (Table 1) is a control experiment where the reactor is fully loaded but remains at room temperature. The purpose of this control experiment is to determine how much hemin, even with no HTL reaction, will dissolve in the blank oil and solvents used and appear in the oil recovered

from the reactor. The iron concentration in the hemin oil in Run 34 ((29 ± 9) ppm) is comparable to that in Runs 1 and 2, which is consistent with hemin not breaking down at 200 °C or 250 °C. Rather, the data indicate that hemin starts decomposing by 300 °C, where the oil phase contained about 1600 ppm of iron. At 350 °C, the iron content in the crude oil is about three times higher, indicating a more extensive decomposition of hemin in the subcritical water at the higher temperature. At 400 °C (Run 6), the iron content is lower than that at 350 °C but still much higher than that at 300 °C. The reduction in iron content at the supercritical temperature could indicate that the iron molecules in the oil break down at 400 °C and form solid products that no longer appear in the oil. In summary, hemin did not decompose below 250 °C and the porphyrin fragments in the HTL oil are not stable at higher temperatures (e.g., 400 °C).

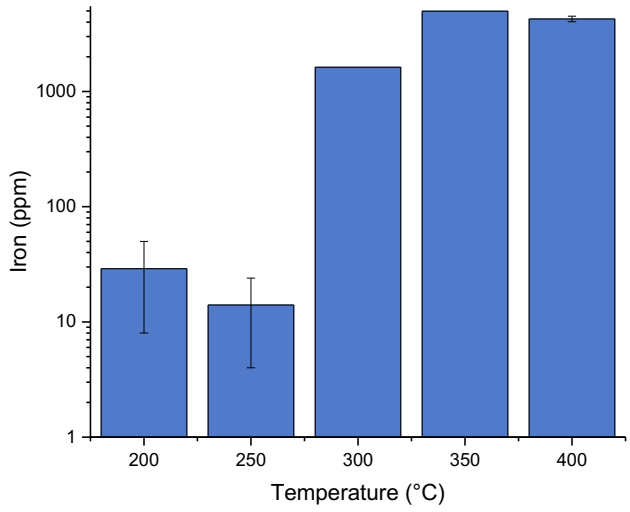

Figure 2: Iron concentration (ppm) in oil from HTL of hemin for 60 min at different temperatures. Solvent is DCM.

3.2 Effect of holding time

Figure 3 illustrates the effect of holding time on the iron concentration in the oil from HTL of hemin at 400 °C. At 3 min (Run 5), the iron content in the crude oil already exceeds 3000 ppm. As the holding time increases, the iron concentration increases to about 4300 ppm at 60 min and then decreases to about 2600 ppm. This temporal variation demonstrates that when the HTL temperature is high enough, hemin will decompose quickly, produce a maximum iron concentration in the oil phase, and then iron-containing molecules in the oil phase will slowly decompose as time increases.

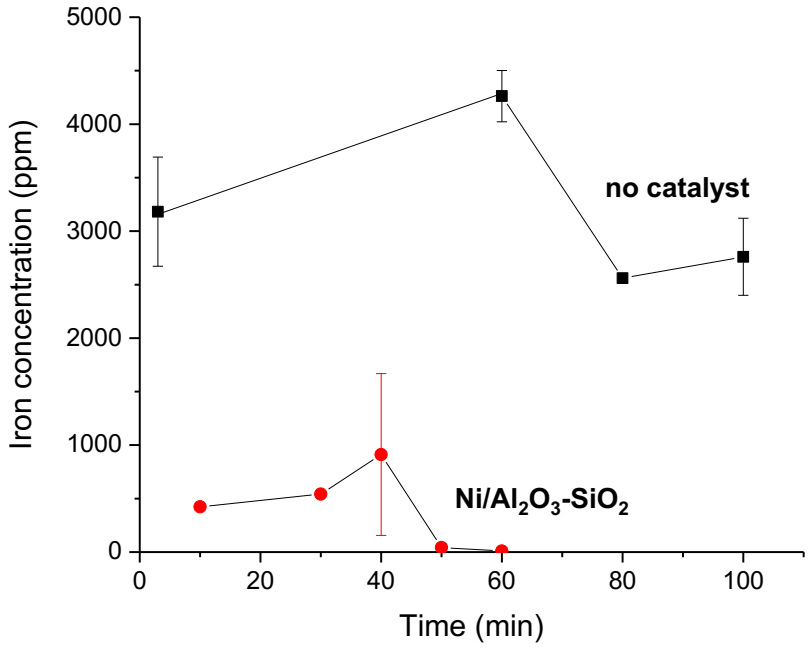

Figure 3: Effect of holding time on iron concentration (ppm) in oil from hemin HTL at 400 °C. Solvent is DCM.

The effect of holding time on HTL in the presence of the Ni/Al_2O_3-SiO_2 catalyst is also shown in Fig. 3 (Runs 27 – 31). In the presence of the catalyst, the iron content in the oil is

reduced to a fraction of its original value. Still, there are hundreds of ppm of iron in the oil phase. However, when the holding time is 50 min or longer, almost all of the iron is removed from the oil via catalytic HTL.

3.3 Effect of heterogeneous catalysts and solvents

In this section, we examine catalysts that were effective for algal biocrude oil demetallation during HTL. [8] The effect of using activated carbon on the iron concentration is shown in Runs 10 - 17. After HTL for 60 min, activated carbon at 25 wt% loading can reduce the iron content to 3080 ppm (Run 12) from its value of 4260 ppm with no added material (Run 6). A higher carbon loading (Runs 14, 15) provides no additional reduction in the iron concentration in the HTL-derived oil. However, with the use of MTBE as a solvent for the oil, the iron concentrations are lower. Nearly all of the iron in the oil phase is eliminated when the catalyst loading is the same as the hemin loading (Run 17) and MTBE is used. Using MTBE in place of DCM also reduces the iron concentration in oil from HTL of hemin with no catalyst (Runs 6 and 9). The addition of Ru supported on activated carbon (Run 32) gives about the same iron content as activated carbon alone.

The effect of a $CoMo/Al_2O_3$ on the iron concentration is shown in Runs 18 - 23. The ability of $CoMo/Al_2O_3$ to reduce the metal concentration is comparable to that of activated carbon. Similarly, increasing the $CoMo/Al_2O_3$ loading and using MTBE as a recovery solvent reduces the iron concentration in the HTL oil (Run 23).

The effect of Ni/Al_2O_3-SiO_2 on the iron concentration is shown in Runs 24 - 31. Ni/Al_2O_3-SiO_2 is the only material tested that is able to remove nearly all the iron in the crude oil with a 25 wt% loading and DCM as solvent (Run 31). Both reaction temperature and holding

time have significant effects on catalytic demetallation using Ni/Al_2O_3-SiO_2. For the same holding time of 60 min and the same catalyst loading of 25 wt%, the iron concentration is reduced to ~ 30% of its value from uncatalyzed HTL at 300 °C (Run 24) and 350 °C (Run 25). At 400 °C, almost all of the iron in the crude oil is removed.

Although the Ni/Al_2O_3-SiO_2 catalyst can be effective in demetallation, there were thousands of ppm of Ni in the resulting oil. Jocz et al. [21] tested the hydrothermal stability of Ni in batch reactors at 400 °C for 60 min, and detected oxidation and dissolution of this metal in the supercritical water. Thus, if one uses a Ni catalyst for hydrothermal demetallation, there will be a trading of Ni for Fe in the oil. An assessment of all the results in Table 1 suggests that using MTBE and a high loading of activated carbon would be a good combination to reduce the iron content in the hemin-derived oil without introducing other metals.

Figure 4 provides SEM images of the solids recovered by DCM after HTL with activated carbon and with Ni/Al_2O_3-SiO_2. Iron is present across the entire surface for both sets of solids, which indicates that iron did deposit on the solids. Table 2, which shows the EDS results for the solids, indicates that iron is uniformly distributed in the solids and the third most abundant element after C and O. The high carbon content in the solids from the run with the Ni catalyst must originate from hemin and indicates that the post-HTL solids contain more than simply the spent catalyst.

Table 2: Elemental compositions of post-HTL (400 °C, 60 min) solids and hemin reactant

	Activated Carbon		Ni/Al_2O_3-SiO_2		Hemin	
Element	wt %	Atomic %	wt %	Atomic %	wt %	Atomic %
C	77.8	85.12	68.74	80.44	62.64	44.74

N			2.21	2.22	8.59	5.26
O	15.8	13.06	15.61	13.72	9.82	5.26
Fe	5.91	1.4	5.03	1.27	8.57	1.32
Ni			7.05	1.69		

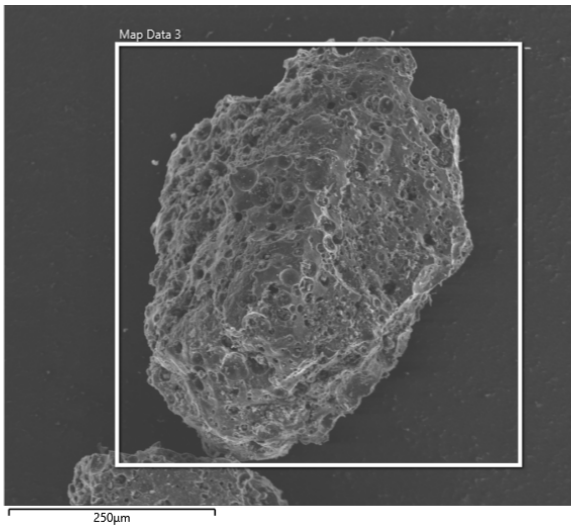

(a)

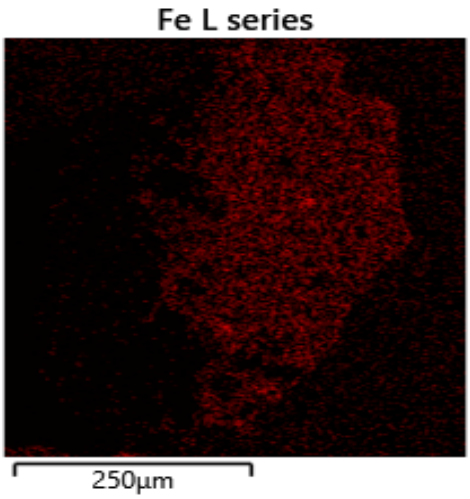

(b)

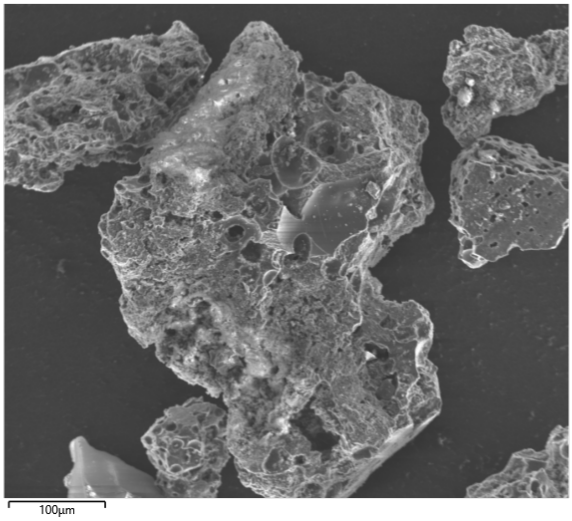

(c)

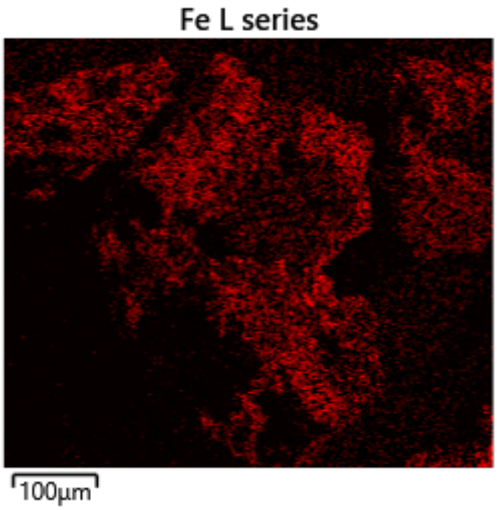

(d)

Figure 4: SEM images of solids (left) and their iron mapping (right) from HTL (400 °C, 60 min) of hemin. Images (a) and (b) are from HTL with activated carbon. Images (c) and (d) are from HTL with Ni/Al_2O_3-SiO_2.

3.4 Comparison with microalgae

A previous study [1] showed that the iron content in algal HTL biocrude was always above 1000 ppm even from a run at a set point temperature of 350 °C with just 1 min of holding time, where the fluid in the reactor reached only about 200 °C. The present results, however, show that hemin does not decompose until the temperature exceeds 250 °C. This difference in iron liberation tendencies could be due to other molecules in microalgae affecting the behavior of heme reactions under hydrothermal conditions or to non-porphyrin forms of iron in microalgae, such as Fe-S clusters, transferring iron into the oil-soluble products.

The iron concentration in the oil from hemin HTL first increasing and then decreasing with longer holding times is consistent with the temporal variation observed for the iron concentration in biocrude from microalgae HTL. [1] More severe processing conditions (higher temperature and longer holding time) facilitate iron reduction for both microalgae and hemin crude oil.

As for the catalytic effects, Ni/Al_2O_3-SiO_2 reduces most of the iron from hemin crude oil and from algal crude oil. Activated charcoal can moderately reduce iron concentrations in algal crude oil. However, with a high loading equivalent to the biomass, activated charcoal can be very effective at reducing the iron concentrations in hemin oil. $CoMo/Al_2O_3$, in comparison, can moderately reduce the iron concentration in hemin oil but is very effective in reducing iron concentrations in algal oil. Thus, different catalysts may perform differently for hemin and for microalgae.

3.5 Molecular characterization of products from HTL of hemin

To characterize the products from HTL of hemin alone, we conducted hydrothermal reaction experiments with no blank oil. The reactors contained only hemin, water, and, at times, the Ni/Al_2O_3-SiO_2 catalyst. The reaction condition was 400 °C and 60 min. The products were analyzed by GC-MS and by FT-ICR-MS. Since no blank oil was used in these experiments, the products are all from HTL of hemin.

Figure 5 displays the total ion chromatogram (TIC) of the hemin oil from HTL with (blue) and without (black) the catalyst. One new peak generated when using the catalyst is a long-chain alkene product with retention time of 19.523 min. Otherwise, catalytic HTL of hemin does not generate many molecules (peaks) that differ from those produced in the non-catalytic reactions.

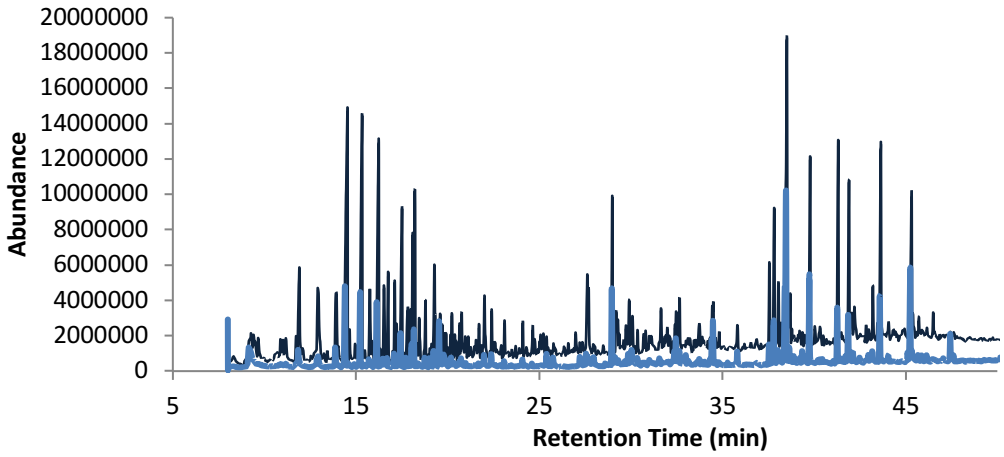

Figure 5: Total ion chromatogram of products from HTL of hemin at 400 °C and 60 min with (blue) and without (black) 25 wt% Ni/Al_2O_3-SiO_2 catalyst

Table 1 in the Supplementary Material provides tentative identities of several major peaks in the TIC. The components include cyclopentenone and cyclohexenone derivatives, indoles, long-chain alcohols, aromatics, and amides. We hypothesize that supercritical water can

attack the methene bridges of the tetrapyrrole rings and produce various pyrrole products in addition to releasing iron through hydroxylation. The pyrrole fragments can then undergo denitrogenation and oxidation reactions to form products such as cyclopentenone and cyclohexenone derivatives.

FT-ICR MS has been used previously to analyze bio-oil from HTL of microalgae, [2,22–24] and Jarvis et al. [2] identified iron porphyrinic species in the algal biocrude oil. Kaczorowska et al.[25] used Electron Induced Dissociation tandem mass spectrometry and observed charged iron (III) complexes. In the present work, FT-ICR MS was used to identify iron-containing products in the oil phase from hemin HTL.

Figure 6 compares the positive ion ESI FT-ICR mass spectra of HTL oil without (top) and with (bottom) the Ni catalyst. More than 15,000 unique molecular formulae were identified in each of the hemin oil samples. In comparison, Faeth et al. [24] identified over 25,000 unique molecular formulae in biocrude samples from fast and isothermal HTL of microalgae. The iron porphyrin structures at m/z 400-500 and at 850 - 1000 after HTL of hemin without catalyst are nearly absent in the spectrum from HTL with the added catalyst. Instead, the dominant species in the products from catalytic HTL of hemin are at m/z 200-400. The products in this range contain many compounds with no iron and two nitrogen atoms (N_2 species). See Table 2 in the Supplementary Material for the details. This elimination of iron porphyrinic species in the oil from catalytic HTL is consistent with the micrographs presented earlier showing Fe decorating the surface of the catalyst and solids remaining after HTL. The iron-porphyrin structures appear to be undergoing reactions and the iron depositing on the catalyst. Jarvis et al. [2] compared FT-ICR spectra of HTL biocrude from cyanobacteria HTL before and after hydroprocessing, and also noted that the porphyrin structures that are dominant in the original HTL biocrude are not

present in the hydroprocessed material. These observations collectively lead to the conclusion that porphyrinic iron in algal biocrude and in hemin oil has similar reaction pathways and fates. Both our previous study on algal biocrude demetallation [8] and Jarvis et al. [2] concluded the mechanisms for iron porphyrin degradation might be similar to those for the nickel and vanadium porphyrins in petroleum crude oil, where the porphyrin structure is first hydrogenated and then hydrogenolysis results in demetallation. [19,26]

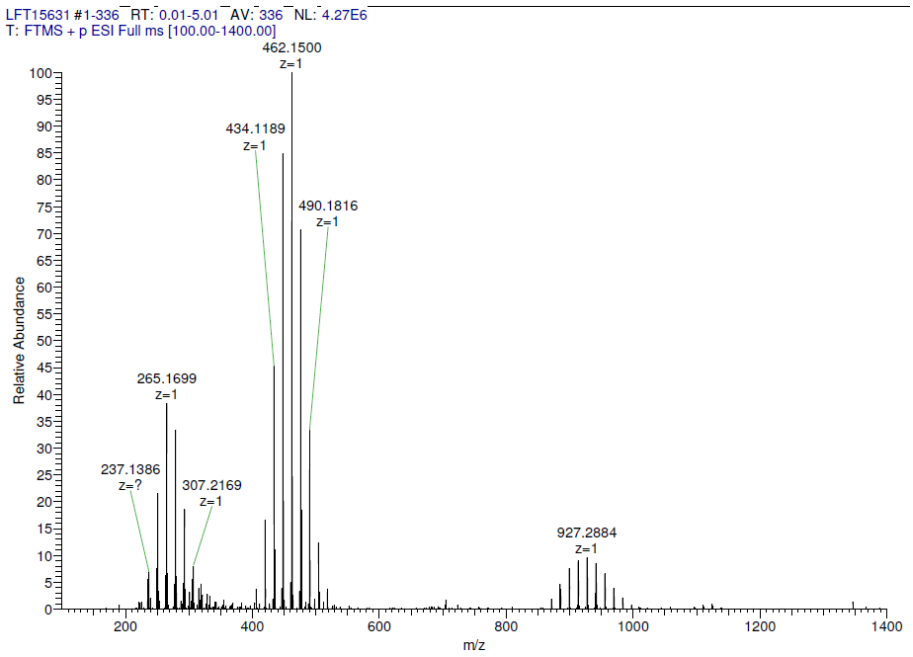

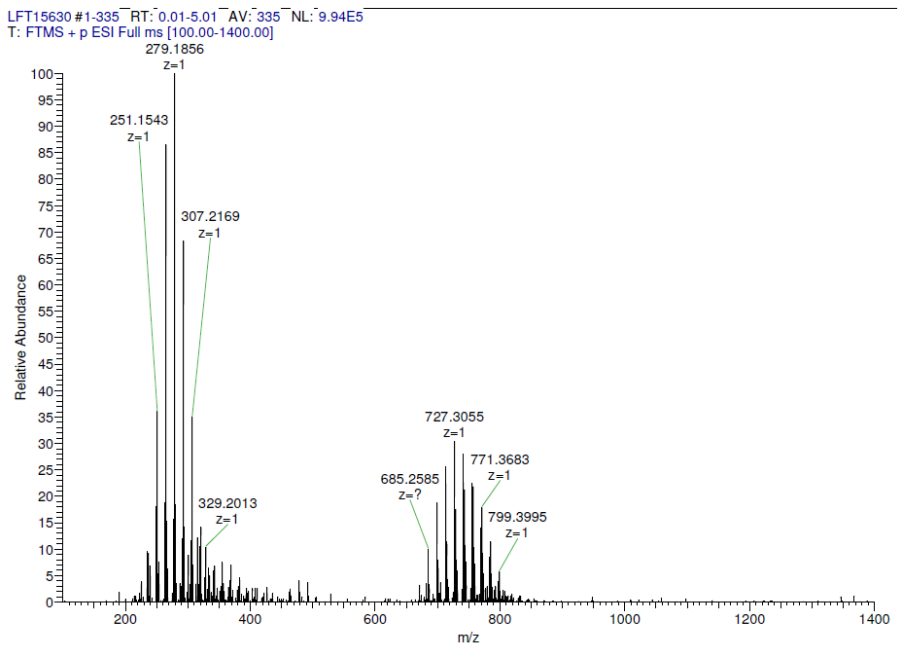

Figure 6: ESI FT-ICR mass spectra of the hemin oil from uncatalyzed (top) and 25 wt% Ni/Al_2O_3-SiO_2 catalyzed (bottom) HTL at 400 °C and 60 min.

Table 3 in the Supplementary Material shows the iron porphyrin molecular formulae assigned to several FT-ICR peaks from hemin HTL crude oil without catalysts. We used the mass spectrum library from Jarvis et al. [2] and identified 52 iron porphyrin ions in the crude oil. The dominant iron porphyrin species are N_4Fe_1 species such as $C_{27}H_{26}N_4Fe_1^+$ at m/z 462.1500, $C_{26}H_{24}N_4Fe_1^+$ at m/z 448.1344, $C_{28}H_{28}N_4Fe_1^+$ at m/z 476.1658, and $C_{29}H_{30}N_4Fe_1^+$ at m/z 490.1816. $N_{4\text{-}6}O_{0\text{-}3}Fe_1$ species were also identified. Those iron-containing porphyrin ions identified in hemin crude oil are similar to those identified in algal biocrude, indicating the utility of using hemin as a model compounds to study iron fates during HTL of microalgae.

4. Summary and Conclusions

Hemin did not decompose into DCM-soluble compounds until the temperature of the hydrothermal environment exceeded 250 °C. The iron concentration in the oil from hemin HTL first increases and then decreases with increasing reaction temperature and holding time. This behavior indicates that hemin decomposes to form smaller iron porphyrinic fragments that are soluble in DCM (oil phase) and then these iron-containing compounds degrade further at more severe conditions and ultimately deposit onto the solid phase. Hydrothermal reaction products include cyclopentenone and cyclohexenone derivatives, indoles, long-chain alcohols, aromatics, amides, and many unique iron-containing porphyrins, with N_4Fe_1 being the most abundant.

Using a Ni/Al_2O_3-SiO_2 catalyst during HTL removed almost all of the iron in the oil from hemin HTL, but the resulting oil has a high nickel content. The combination of using MTBE as the solvent and using activated carbon during HTL could also remove most of the iron in the oil from hemin HTL, without adding new metals to it. The porphyrin structures that are dominant in the oil from hemin HTL are much less abundant when using the Ni catalyst during HTL, suggesting that those iron porphyrin molecules have undergone ring opening and degradation with the introduction of the catalyst.

Finally, the results reported herein regarding the behavior of iron in oil from hemin HTL are in general agreement with those reported for HTL of microalgae.

Acknowledgement

We thank Penn State staff scientist Julie Anderson for assistance with the SEM-EDS characterization. We thank Zhongrui Zhou at UC Berkeley for analyzing samples using FT-ICR-MS. We thank Prof. Rob Rioux for access to the ICP-OES.

References

[1] J. Jiang, P.E. Savage, Metals and Other Elements in Biocrude from Fast and Isothermal Hydrothermal Liquefaction of Microalgae, Energy & Fuels. 32 (2017) 4118–4126. doi:10.1021/acs.energyfuels.7b03144.

[2] J.M. Jarvis, N.M. Sudasinghe, K.O. Albrecht, A.J. Schmidt, R.T. Hallen, D.B. Anderson, J.M. Billing, T.M. Schaub, Impact of iron porphyrin complexes when hydroprocessing algal HTL biocrude, Fuel. 182 (2016) 411–418. doi:10.1016/j.fuel.2016.05.107.

[3] J.P. Dunn, H.G. Stenger, I.E. Wachs, Molecular structure-reactivity relationships for the oxidation of sulfur dioxide over supported metal oxide catalysts, Catal. Today. 53 (1999) 543–556. doi:10.1016/S0920-5861(99)00142-X.

[4] Z. Yuxia, D. Quansheng, L. Wei, T. Liwen, L. Jun, Chapter 13 Studies of iron effects on FCC catalysts, Stud. Surf. Sci. Catal. 166 (2007) 201–212. doi:10.1016/S0167-2991(07)80196-0.

[5] D. Wallenstein, D. Farmer, J. Knoell, C.M. Fougret, S. Brandt, Progress in the deactivation of metals contaminated FCC catalysts by a novel catalyst metallation method, Appl. Catal. A Gen. 462–463 (2013) 91–99. doi:10.1016/j.apcata.2013.02.002.

[6] Y. Mathieu, A. Corma, M. Echard, M. Bories, Single and combined Fluidized Catalytic Cracking (FCC) catalyst deactivation by iron and calcium metal-organic contaminants, Appl. Catal. A Gen. 469 (2014) 451–465. doi:10.1016/j.apcata.2013.10.007.

[7] H. Gao, G. Wang, C. Xu, J. Gao, Eight-lump kinetic modeling of vacuum residue catalytic cracking in an independent fluid bed reactor, Energy and Fuels. 28 (2014) 6554–6562. doi:10.1021/ef501260n.

[8] J. Jiang, P.E. Savage, Influence of process conditions and interventions on metals content in biocrude from hydrothermal liquefaction of microalgae, Algal Res. 26 (2017) 131–134. doi:10.1016/j.algal.2017.07.012.

[9] M.A. Borowitzka, J.A.R. Editors, The Physiology of Microalgae, 2016.

[10] M. Gledhill, The determination of heme b in marine phyto- and bacterioplankton, Mar. Chem. 103 (2007) 393–403. doi:10.1016/j.marchem.2006.10.008.

[11] E. Nagababu, J.M. Rifkind, Heme Degradation by Reactive Oxygen Species, Antioxid. Redox Signal. 6 (2004) 967–978. doi:10.1089/ars.2004.6.967.

[12] Y. Zhu, R.B. Silverman, Electronic effects of peripheral substituents at porphyrin meso positions, J. Org. Chem. 72 (2007) 233–239. doi:10.1021/jo061951j.

[13] R. Bonnett, G.F. Stephenson, The meso Reactivity of Porphyrins and Related Compounds. I. Nitration, J. Org. Chem. 30 (1965) 2791–2798. doi:10.1021/jo01019a070.

[14] R. Bonnett, I.A.D. Gale, G.F. Stephenson, The meso-reactivity of porphyrins and related compounds. Part II. Halogenation, J. Chem. Soc. C Org. (1966) 1600–1604. doi:10.1039/j39660001600.

[15] R. Bonnett, A.F. McDonagh, The meso-reactivity of porphyrins and related compounds. Part VI. Oxidative cleavage of the haem system. The four isomeric biliverdins of the IX series, J. Chem. Soc. Perkin Trans. 1. (1973) 881–888. doi:10.1039/P19730000881.

[16] K. Welter, E. Salazar, Y. Balladores, O.P. Márquez, J. Márquez, Y. Martínez, Electrochemical removal of metals from crude oil samples, Fuel Process. Technol. 90 (2009) 212–221. doi:10.1016/j.fuproc.2008.09.004.

[17] H. Shang, Y. Liu, J.-C. Shi, Q. Shi, W.-H. Zhang, Microwave-assisted nickel and vanadium removal from crude oil, Fuel Process. Technol. 142 (2016) 250–257.

doi:10.1016/j.fuproc.2015.09.033.

[18] P.C. Mandal, M. Sasaki, M. Goto, Nickel removal from nickel etioporphyrin (Ni-EP) using supercritical water in the absence of catalyst, Fuel Process. Technol. 104 (2012) 67–72. http://linkinghub.elsevier.com/retrieve/pii/S0378382011002591 (accessed June 29, 2016).

[19] J. Wei, R. Agrawal, Hydrodemetalation of Nickel and Vanadium Porphyrins. 1. Intrinsic Kinetics, Ind. Eng. Chem. Process Des. Dev. 23 (1984) 505–514. doi:10.1021/i200026a017.

[20] C.A. Savastano, The solvent extraction approach to petroleum demetallation, Fuel Sci. Technol. Int. 9 (1991) 855–871. doi:10.1080/08843759108942300.

[21] J.N. Jocz, L.T. Thompson, P.E. Savage, Catalyst Oxidation and Dissolution in Supercritical Water, Chem. Mater. 30 (2018) 1218–1229. doi:10.1021/acs.chemmater.7b03713.

[22] N. Sudasinghe, B. Dungan, P. Lammers, K. Albrecht, D. Elliott, R. Hallen, T. Schaub, High resolution FT-ICR mass spectral analysis of bio-oil and residual water soluble organics produced by hydrothermal liquefaction of the marine microalga Nannochloropsis salina, Fuel. 119 (2014) 47–56. doi:10.1016/j.fuel.2013.11.019.

[23] M.M. Sanguineti, N. Hourani, M. Witt, S.M. Sarathy, L. Thomsen, N. Kuhnert, Analysis of impact of temperature and saltwater on Nannochloropsis salina bio-oil production by ultra high resolution APCI FT-ICR MS, Algal Res. 9 (2015) 227–235. doi:10.1016/j.algal.2015.02.026.

[24] J.L. Faeth, P.E. Savage, J.M. Jarvis, A.M. Mckenna, P.E. Savage, Characterization of products from fast and isothermal hydrothermal liquefaction of microalgae, AIChE J. 62

(2016) 815–828. doi:10.1002/aic.15147.

[25] M.A. Kaczorowska, H.J. Cooper, Electron induced dissociation (EID) tandem mass spectrometry of octaethylporphyrin and its iron(iii) complex, Chem. Commun. 47 (2011) 418–420. doi:10.1039/c0cc02198a.

[26] R.A. Ware, J. Wei, Catalytic hydrodemetallation of nickel porphyrins. I. Porphyrin structure and reactivity, J. Catal. 93 (1985) 100–121. doi:10.1016/0021-9517(85)90155-1.

SUPPORTING INFORMATION

Table 1: Potential identities for some major peaks in total ion chromatogram from hemin HTL crude oil. Multiple identities are listed for peaks when multiple library compounds gave comparable similarity indexes

Retention time (min)	NIST MS Library Hit	Similarity Index
11.906	2-Cyclopenten-1-one, 3-methyl-	94
	2,4-Dimethylfuran	90
12.908	2-Cyclopenten-1-one, 3,4-dimethyl-	86
	2,4-Hexadiene, 2,3-dimethyl-	83
	4,4-Dimethyl-2-cyclopenten-1-one	83
13.926	2-Cyclopenten-1-one, 3,4-dimethyl-	92
	4.4-DImethyl-2-cyclopenten-1-one	89
	2,4-Hexadiene, 2,3-dimethyl-	87
14.528	2-Cyclopenten-1-one, 2,3-dimethyl-	95
	2-Cyclopenten-1-one, 3,4-dimethyl-	86
15.326	2-Cyclopenten-1-one, 3,4,4-trimethyl-	89
	Phenol, 2-methoxy-	88
16.232	Ethanone, 1-(1-cyclohexen-1-yl)-	88
	Phenol, 2-methoxy-	86
17.503	5-Ethylcyclopent-1-enecarboxaldehyde	85
	1,3-Hexadiene, 3-ethyl-2-methyl-, (Z)-	85
	Cyclohexane, (1-methylethylidene)-	85
	Cyclohexanone, 3-ethenyl-	85
18.082	1,3-Hexadiene, 3-ethyl-2,5-dimethyl-	84
	2-cyclopenten-1-one, 2,3,4,5-tetramethyl-	84
18.202	3,7,7-Trimethyl-8-(2-methyl-propenyl)-bicyclo[4.2.0]oct-2-ene	77
	2-Cyclohexen-1-one, 5-methyl-2-(1-methylethyl)-	75
19.523	3-tetradecene, (E)-	94
	1-Dodecene	94
	3-Tetradecene, (Z)-	93
	3-Hexadecene, (Z)-	93
27.617	1H-Indole, 2,6-dimethyl-	91
	1H-Indole, 2,3-dimethyl-	93
	1H-Indole, 2,5-dimethyl-	91
28.971	1-Dodecanol	94
	Methyl 4, 6-decadienyl ether	92
38.496	Benzene, 1,3,5-tris(3-methyl-3-butenyl)-	68
39.765	1,6-Heptadiene, 2-methyl-6-phenyl-	66
41.298	4,5-Diphenylocta-1,7-diene(dl)	74
43.624	1-Phenylcyclopentanecarboxylic acid	73
45.227	9-Octadecenamide, (Z)-	92

Table 2: Molecular formulae of dominant species in FTICRMS spectra at m/z 200-400 from both uncatalyzed and catalyzed HTL of hemin at 400 °C and 60 min.

Formula	Theoretical mass	Experimental Mass
C16H15N2	235.1230	235.1237
C16H17N2	237.1386	237.1394
C17H17N2	249.1386	249.1394
C17H19N2	251.1543	251.1551
C18H19N2	263.1543	263.1551
C18H20N2	264.1621	264.1629
C18H21N2	265.1699	265.1708
C18H22N2	266.1733	266.1786
C18H22N2	266.1733	266.1786
C19H21N2	277.1699	277.1708
C19H23N2	279.1856	279.1865
C19H24N2	280.1890	280.1943
C20H25N2	293.2013	293.2021
C20H26N2	294.2046	294.2100
C21H25N2	305.2013	305.2021
C21H27N2	307.2169	307.2178
C22H23N2	315.1857	315.1865
C22H29N2	321.2326	321.2335

Table 3: Molecular formulae of iron porphyrins from uncatalyzed HTL of hemin at 400 °C and 60 min. Double bond equivalents (DBE) and theoretical mass are from Jarvis et al. [1]

Formula	DBE	Theoretical Mass	Experimental mass
C26H24N4Fe1	17.5	448.134486	448.1344
C27H24N4Fe1	18	461.142311	461.1423
C27H26N4Fe1	17.5	462.150136	462.1500
C28H26N4Fe1	18.5	474.150136	474.1504
C28H26N4Fe1	18	475.157961	475.1562
C28H28N4Fe1	17.5	476.165786	476.1658
C29H28N4Fe1	18.5	488.165786	488.1661
C29H30N4Fe1	17.5	490.181436	490.1816
C30H28N4Fe1	19	501.173611	501.1794
C30H30N4Fe1	18.5	502.181436	502.1818
C30H32N4Fe1	17.5	504.197086	504.1972
C29H28N4O1Fe1	18	505.168526	505.1638
C28H28N6Fe1	18	505.179759	505.1711
C30H32N4Fe1	17	505.204911	505.2006
C29H31N5Fe1	17	506.20016	506.2041
C28H30N6Fe1	17	507.195409	507.1977
C31H30N4Fe1	19.5	514.181436	514.1990
C30H29N5Fe1	19	516.18451	516.1848
C31H32N4Fe1	18.5	516.197086	516.1971
C30H30N4O1Fe1	18.5	518.176351	518.1716
C31H34N4Fe1	17.5	518.212736	518.2129
C30H30N4O1Fe1	18	519.184176	519.1822
C32H28N4Fe1	21.5	524.165786	524.1665
C32H34N4Fe1	18.5	530.212736	530.2172
C32H36N4Fe1	17.5	532.228386	532.2291
C31H32N4O1Fe1	18	533.199826	533.2003
C30H32N6Fe1	18	533.211059	533.2187
C30H30N4O2Fe1	18.5	534.171265	534.1773
C33H30N4Fe1	21.5	538.181436	538.1819
C31H32N4O2Fe1	18	549.19474	549.2021
C34H32N4Fe1	21.5	552.197086	552.1975
C34H36N4Fe1	19.5	556.228386	556.2281
C34H36N4Fe1	19	557.236211	557.2323
C34H38N4Fe1	18.5	558.244036	558.2417
C32H32N4O2Fe1	19.5	560.186915	560.1898
C32H32N4O2Fe1	19	561.19474	561.1917
C35H34N4Fe1	21.5	566.212736	566.2130
C35H38N4Fe1	19.5	570.244036	570.2458

C33H32N4O2Fe1	20	573.19474	573.1923
C33H37N5O1Fe1	18.5	575.2342	575.2304
C36H36N4Fe1	21.5	580.228386	580.2279
C36H40N4Fe1	19.5	584.259686	584.2530
C34H37N5O1Fe1	19.5	587.2342	587.2325
C33H36N4O3Fe1	18.5	592.21313	592.2102
C37H38N4Fe1	21.5	594.244036	594.2466
C36H40N4O1Fe1	19.5	600.254601	600.2567
C37H44N4Fe1	18.5	600.290986	600.2974
C36H42N4O1Fe1	18.5	602.270251	602.2769
C35H40N4O2Fe1	18.5	604.249516	604.2516
C34H38N4O3Fe1	18.5	606.22878	606.2303
C38H38N4Fe1	22.5	606.244036	606.2471
C37H43N5O1Fe1	19.5	629.28115	629.2888

Reference

[1] J.M. Jarvis, N.M. Sudasinghe, K.O. Albrecht, A.J. Schmidt, R.T. Hallen, D.B. Anderson, J.M. Billing, T.M. Schaub, Impact of iron porphyrin complexes when hydroprocessing algal HTL biocrude, Fuel. 182 (2016) 411–418. doi:10.1016/j.fuel.2016.05.107.